REPORT DOCUMENTATION PAGE

Form Approved
OMB NO. 0704-0188

1. AGENCY USE ONLY (Leave Blank)	2. REPORT DATE	3. REPORT TYPE AND DATES COVERED
	March 29, 2001	Final Progress, 15Jan97- 31 Dec00

4. TITLE AND SUBTITLE
Tropospheric Lidar: Development of Techniques and Practical Measurements

5. FUNDING NUMBERS
DAAG-55-97-1-0297

6. AUTHOR(S)
T.D. Wilkerson, V.B. Wickwar, M.R. Hammond

7. PERFORMING ORGANIZATION NAME(S) AND ADDRESS(ES)
Utah State University
Logan, UT 84322

8. PERFORMING ORGANIZATION REPORT NUMBER
N/A

9. SPONSORING / MONITORING AGENCY NAME(S) AND ADDRESS(ES)
U. S. Army Research Office
P.O. Box 12211
Research Triangle Park, NC 27709-2211

10. SPONSORING / MONITORING AGENCY REPORT NUMBER
ARO 35034.1-EV

11. SUPPLEMENTARY NOTES
The views, opinions and/or findings contained in this report are those of the author(s) and should not be construed as an official Department of the Army position, policy or decision, unless so designated by other documentation.

12 a. DISTRIBUTION / AVAILABILITY STATEMENT	12 b. DISTRIBUTION CODE
Approved for public release; distribution unlimited.	

13. ABSTRACT (Maximum 200 words)

We report the successful development of a hydrogen Raman shifted tunable narrow line alexandrite laser transmitter for near-IR H_2O spectroscopy. Fourier analysis of the the alexandrite laser radiation showed a 10 MHz fundamental linewidth and 20 MHz raman linewidth. As a first test of the transmitter we measured the line strengths and air-broadened widths for 15 lines in the 1140 nm water vapor band. These lines were measured by transmittance of the laser beam through a 55 meter long White cell. The results are compared to the HITRAN-2000 database. Relative to this database, our observed line strengths are larger by a factor of 1.28 (±13%) on average, and the line widths by 1.13 (±21%). Precisions vary from line to line, so these are only representative comparisons to HITRAN-2000. Detailed results for all 15 lines studied are presented. We also present all preliminary work that was done for the development of the system. This research is supported by the US Army Research Office. Purchase of the alexandrite laser was made possible by a grant from the National Science Foundation.

14. SUBJECT TERMS	15. NUMBER OF PAGES
Atmospheric Lidar, Water Vapor, Temperature, Alexandrite Laser, Water Vapor Spectra Line Strengths, Line Widths, HITRAN	35
	16. PRICE CODE

17. SECURITY CLASSIFICATION OR REPORT	18. SECURITY CLASSIFICATION ON THIS PAGE	19. SECURITY CLASSIFICATION OF ABSTRACT	20. LIMITATION OF ABSTRACT
UNCLASSIFIED	UNCLASSIFIED	UNCLASSIFIED	UL

Table of Contents

Statement of Problem Studied ii

Summary of Most Important Results ii

Chapter
I. Introduction 1
II. Background and Theory 3
III. Results and Discussion 5
A. Experimental Description 5
1. Diode Laser 5
2. Alexandrite Laser 8
3. Frequency Conversion 8
B. Water Vapor Measurements 9
C. Comparisons to HITRAN-2000 10
D. Error Analysis 12
IV. Conclusions 13

Bibliography 16

Figures 18

Listing of All Publications and Reports 29

Listing of All Participating Scientific Personnel 29

Report of Inventions 29

Statement of Problem Studied

Lidar profiling of atmospheric water vapor must be done with Differential Absorption Lidar (DIAL) in the near infrared in order to work in daylight and over a wide range of humidity. The near IR is essential in order to obtain a range of water vapor line strengths, and opens up the capability for temperature profiling as well. High laser power and accurate spectral line parameters are essential for accurate DIAL profiling.

Summary of Most Important Results

We have developed a tunable laser method for getting appropriate power and line width for H_2O-DIAL work at 1140 nm, using a diode injection-stabilized alexandrite laser Raman-shifted in H_2. The success of this method also implies the accessibility of the 940 nm water band for H_2O-DIAL, by Raman-shifting in D_2.

The first important application of this development has been to make new measurements of H_2O line strengths (S) and line widths (γ) for selected lines in the 1140 nm band, covering a range of lower state excitation energy. This work joins with an increasing number of efforts in the atmospheric community to review and correct the near IR data for H_2O in the HITRAN database. For 15 lines in the wavenumber range 8865 – 8915 cm^{-1}, we find that the line strengths compared to HITRAN-2000 are a factor of 1.28 (± 13%) larger on average, and the line width ratios are 1.13 (± 21%).

This work lays a solid foundation for greatly improved H_2O line parameter measurements in both the 940 nm and 1140 nm bands, and for DIAL profiling of humidity and temperature in the atmosphere. Plans and suggestions for continued research on these topics have been communicated to the US Army Research Office.

In addition to the main line of research under this contract, numerical and experimental studies were undertaken to explore the possible application of laser/lidar methods lying within our areas of expertise to existing R&D programs in the DoD, and to areas of perceived threats to Army operations.

Tunable diode lasers needed for injection control of the alexandrite laser are operated over the wavelength range 760 – 780 nm, and are frequency-locked on absorption lines of atomic rubidium (780 nm) and potassium (770 nm) and molecular oxygen (762 – 769 nm). The diode laser line width is < 100 kHz.

Atmospheric temperatures in a closed optical path are measured using the absorption of diode laser light by lines in the oxygen A-band, demonstrating the principle of future lidar temperature measurements in the open atmosphere.

The alexandrite laser operates at a PRF of 20Hz and is well "seeded" (i.e., injection-locked) by the diode laser, so that the alexandrite output is in a low order spatial mode and in a single spectral mode. Diagnostics include a Fabry-Perot analyzer which demonstrates the laser linewidth to be less than 50 MHz, and a Fast Fourier Transform showing a linewidth of order 10 MHz. The alexandrite output is a smooth near-Gaussian pulse of about 200 nsec duration.

The desired light at 1140 nm is generated by Raman-shifting the alexandrite laser output in a 1-meter high pressure H_2 cell. In addition to the first Stokes output at 1140 nm, other Raman components are also generated, *e.g.* 586 nm (first anti-Stokes) and 470 nm (second anti-Stokes). Relative yields of these components are adjusted by varying the cell pressure, laser pulse energy, and beam focusing geometry, so as to optimize the pulse energy obtained in the near IR.

With the present alexandrite laser output coupler, the spectral references employed are the K resonance line at 770 nm and the O_2 lines in the A-band, and the wavenumber range provided by Raman-shifting is 8830 – 8925 cm^{-1}. A different coupler would permit operation at 780 nm (the Rb line reference) and extend the near IR range downward to 8660 cm^{-1}. To go the other way, say to Raman-shifted photon energies of order 9500 cm^{-1}, requires yet another alexandrite output coupler and active control of the laser rod temperature.

The time dependence of the IR pulse is analyzed and demonstrates both a delay and more transient behavior relative to the alexandrite input. Fourier analysis, however, shows that the 1140 nm output has a line width no greater than 20 MHz (< 0.001 cm^{-1}). This is only 0.34 % of the nominal width of H_2O absorption lines at atmospheric pressure, meaning that our laser source is capable of very high resolution measurements of the H_2O line shapes under ambient conditions.

Wavelength registry in the 1140 nm band of H_2O is accomplished by means of the alexandrite's wavelength "position" in the oxygen A-band spectrum around 765 nm, since the Raman line for H_2 is narrow and well defined. Tuning over the H_2O spectrum is controlled by observing the alexandrite wavelength relative to the oxygen lines, and by adding known wavelength "jumps" using the diode laser's frequency control system.

Using a closed, multipass White cell geometry having a pathlength up to 60 meters, we scan the absorption spectrum of laboratory air containing known amounts of water vapor. We identify all the lines by comparison with a synthetic spectrum generated by an atmospheric transmission code that contains database line parameters. This was done using various HITRAN tabulations (1986 through 2000) and a power series representation of the Voigt function that convolutes Doppler and pressure broadening.

Detailed comparison of our measurements and the transmission codes showed systematic differences between the observed and calculated spectra of water vapor. The process was inverted to permit re-evaluation of the line parameters for 15 selected lines. The new line strengths are, on average, a factor of 1.28 (± 13%) higher than claimed in HITRAN-2000, and the line width ratios are 1.13 (± 21%).

These results are consistent with growing evidence that the HITRAN compilations for the near IR lines of H_2O are in need of critical review and further measurements. We have submitted a prospectus for such a research program to the US Army Research Office.

An N_2/H_2O Raman lidar concept based on Raman-shifting has been explored by the Principal Investigator while in residence at the Max Planck Institut in Hamburg. The main principal of this method is to "hide" UV Raman lidar returns within the strong Ca^+ Fraunhofer lines (396.4 and 396.8 nm), to obtain a filtering action against solar background, and thereby support daytime Raman lidar observations of the atmosphere. The search continues for a laser transmitter at the right wavelengths that is also sufficiently powerful for practical use. Background suppression by a factor of 5 – 10 is possible in principle, and would facilitate the daytime applications of Raman lidar.

During the course of our research, we were able to carry out experimental and numerical work in support of DoD research elsewhere and in subject areas pertaining to potential military threats.

USU personnel and our tunable diode laser equipment were loaned to the AFRL/DELC at Kirtland AFB for experiments on detection of molecular oxygen populations in the chemical oxygen-iodine laser (COIL). Vibrationally-excited ground state O_2 was not detected in these experiments.

An on-campus demonstration of remote detection of fluorescent aerosols was carried out using our pulsed YAG laser and PMT detector. Even in this very preliminary trial, we were able to establish a bio-assay cellular equivalent detection limit of 10^6 cells per milliliter for a common type of cellular material. The projected value of useful lidar range at this sensitivity level is 1 kilometer.

We carried out numerical studies of atmospheric effects and target-size effects on the feasibility of laser tracking from a ground-based lidar station, based on intelligence and operational needs for remote tracking and characterization of potentially hostile rockets and satellites. Target shape effects were also calculated, taking into account the well-known transition from $1/R^2$ to $1/R^4$ signal dependence as a finite-size target recedes from the lidar station. Target distances of 1000 kilometers are practical for modest lidar transmitters.

I. Introduction

A number of new or improved approaches to lidar remote sensing of the troposphere are now possible owing to advances in laser technology and new techniques in the last decade. Of particular importance to atmospheric measurements is the *DI*fferential *A*bsorption *L*idar technique where multichannel laser remote sensing allows direct temperature and density profiling given *a priori* knowledge of molecular line parameters. In this work, we have concentrated our efforts on the development of a broadly tunable (100 nm) near-infrared laser transmitter having a sufficiently narrow line width to measure the absorption lines of H_2O, O_2, and metallic species of the troposphere, stratosphere, and mesosphere. We used this new platform to measure H_2O line parameters and compared the results to the current *Hi*gh-resolution *Tran*smission database (HITRAN). The database, regarded as the industry standard in molecular line parameter compilation, is important to the successful operation of any DIAL system.

The diode seeded alexandrite ring laser lies at the heart of our platform. The suitability of this laser as the preferred light source for H_2O and O_2 DIAL observations has recently been demonstrated by *Wulfmayer et al* [*1995*]. The O_2 bands near 730 nm and 760 nm occur within the fundamental output range (720-800 nm) of the laser; the H_2O bands near 940 and 1140 nm are accessed through hydrogen Raman conversion. The 940 and 1140 nm bands are particularly important for laser remote sensing because certain lines in the rotational manifold are sufficiently strong to impact lidar measurements of temperature and humidity.

We also investigated other approaches to temperature measurement using the atomic transitions of Potassium (D_1 and D_2 lines near 770 and 767 nm) and the O_2 A-band rotational lines (759-770 nm). Potassium is one of several metallic species commonly found in the mesosphere through meteoric deposition. While the K D_2 line is nearly resonant with the $^QP21$ of O_2, the K D_1 line is well suited for direct measurement. The near resonance of K D_2 with O_2 prohibits the use of that line for ground-based temperature profiling since without knowledge of the O_2 column densities, accurate determination of extinction becomes problematic. The recent successes of K mesospheric temperature profiling by experimenters at Arecibo, Puerto Rico and Kühlungsborn, Germany have demonstrated the capability of this approach [*Tepley and Sulzer, 2000; Zahn and Höffner, 1996*]. In our preliminary investigations we confirmed the near resonance of the K D_2 line with O_2 $^QP21$ rotational line and developed a temperature controlled system for a K laboratory source. In practice, a K based transmitter must employ accurate wavelength control through frequency locking methods. The temperature profiling can then be determined by standard DIAL methods.

The spectroscopic measurements of the O_2 A-band afforded an accurate measurement of laboratory temperature. This effort illustrated the advantages and potential for the high-resolution wavelength control of our system. One potential problem with DIAL lidars using the O_2 A-band lines is the redistribution of the lidar return spectrum. Regardless of the transmitter linewidth, the return spectrum is Doppler broadened. Thus the radiative transfer between the transmitted and reflected signal is different. Using broader lines such as H_2O or else pairs of lines for which the effect tends to be similar for both would minimize the influence of this effect on DIAL observation. However, the latter compensation may be compromised by the rotational quantum number dependence of pressure broadening since temperature determination is done mainly through the measurement of the Boltzmann factor between 2 transitions of low and high rotational quantum number. This technique can also be compromised in cases of non-Local Thermodynamic Equilibrium where Boltzmann statistics do not apply.

In 1973 the HITRAN database was first made available to the public and has since then become the standard model for spectroscopic properties of the atmosphere [*Rothman et al., 1988*]. While the spectroscopic parameters for O_2 have been trusted by the community for many years now, recent studies [*Gutman et al., 1990; Belmiloud, 2000; Giver et al., 2000*] have suggested that the quoted values for the near-infrared water lines need to be reconsidered. Historically, water vapor spectral measurements in the near-IR region just beyond 1000 nm are sparse owing to the lack of good light sources and detectors at those wavelengths. There are currently no broadly tunable sources which directly operate in the near-IR so there has been an impetus to develop technology to access this part of the spectrum [*Guerra, 1993*]. Early HITRAN compilations of H_2O lines were constructed mostly from solar spectrum analyses [*Swensson et al., 1970*], and laboratory efforts by Giver et al. in 1982 of the 940 nm band showed good agreement for 97 lines observed [*Giver et al., 1982*]. In 1993, the 940 nm band was measured with a Raman shifted dye laser for comparison with HITRAN-91 version [*Chu et al., 1993*]. In that work, 45 line strengths (6% average uncertainty) and 30 line widths (8% average uncertainty) were measured. The HITRAN-91 line strengths consisted of values measured from solar spectrum analyses [*Chevillard, 1989*] and were found to be in agreement with experiment to 3%. The 30 measured widths were found to be a factor of 1.059 larger on average than the HITRAN-91 values. Historically, experimental comparisons to the HITRAN database have shown favorable agreement for the 940 nm band.

Recent theoretical work in the 1140 nm band has been more controversial. In 1995, intensity calculations made by Lynas-Gray et al. were compared to HITRAN database entries from which it was suggested that the HITRAN intensity errors were thought to be less than 10% in most cases but may be as high 50% in a few cases [*Lynas-Gray et al, 1995*]. The most recent theoretical calculations of line positions and intensities [*Partridge et al., 1997*] provide the most accurate and extensive treatment of the water problem to date. Line positions and intensities for over 30,000 lines were calculated and compared to the HITRAN 96 database. While the total sum of intensities for the calculations were in good agreement with HITRAN, the individual band sums have significant variations. The summed intensities for the lines in the (111-000) vibrational band were reported to be a factor of 1.33 larger than corresponding HITRAN entries. These lines are of interest since our measurements included lines mostly from this band. The overall trend in empirically and theoretically determined line strengths suggests that HITRAN line strengths for H_2O may be under-predicted in the 1140 nm band. Contrary to this trend is the recent work by Giver et al. [*2000*] whose conclusions suggested HITRAN H_2O line strengths were slightly over-predicted.

The most recent literature database on near-IR water vapor line strengths and widths include theoretical predictions, which in some cases are in poor agreement with direct measurements. The present near-IR compilations of line strength data in HITRAN-2000 are those of Giver et al. [*2000*]. This update was motivated by systematic differences found between HITRAN-96 and the corresponding literature used to make up the database. The widths listed for the (111-000) vibrational band are mostly compiled from theoretical work done by Gamache and Davies [*Gamache and Davies; 1983*]. The tabulation of widths in HITRAN are in the form N_2-broadened half widths, self-broadened half widths, and a temperature exponent for N_2-broadening [*Gamache and Rothman; 1988*]. From these line-by-line data, the total width of a line is calculated for a given temperature and pressure. In our work, we did not explore the accuracy of the temperature exponent due to time constraints. Most work on HITRAN validation

has been done at a "reference temperature" which occurs in the HITRAN data base design as a fiduciary temperature (296 K).

We have developed a tunable laser method for getting appropriate power and line width for H_2O-DIAL work at 1140 nm, using a diode injection-stabilized pulsed alexandrite laser Raman shifted in H_2. The first important application of this development has been to make new measurements of H_2O linestrengths and line widths for selected lines from the $2\nu+\delta$ polyad of water vapor at 1140 nm. The measurements cover a range of lower excitation energies. The data were taken under laboratory conditions at Utah State University during October 2000. This work joins with an increasing number of efforts in the atmospheric community to review and correct the near IR data for H_2O in the HITRAN-2000 database. For 15 lines in the wavenumber range 8865-8915 cm^{-1}, we find that the line strengths compared to HITRAN-2000 are a factor of 1.28 (±13%) larger on average, and the line widths comparisons are a factor of 1.13 (±21%) larger on average. Additionally, we explored methods of diode laser wavelength control, which plays a crucial role in high-resolution spectroscopy of the atmosphere with an alexandrite transmitter. These efforts include spectroscopic measurements of temperature, diode laser frequency locking and stabilization, and theoretical modeling of the atmospheric transmittance spectrum. We make an attempt here to illustrate the advantages and potentials for this new technology.

II. Background and Theory

A monochromatic light wave attenuates exponentially in the atmosphere according to the Beer-Lambert law [*Measures, 1984*], which is a function of the absorption coefficient (σ), the number density (ρ) of absorbers, and the distance (x) over which the light wave travels. In the absence of aerosols, the absorption coefficient is a function of atomic and molecular transitions. The atmospheric transmittance at any point in the spectrum is determined by all contributions of atomic and molecular absorption at that frequency,

$$T(\nu) = \exp\left[-x\sum_{i=1}^{N}\rho_i\sigma(\nu,\nu_i)\right] \tag{1}$$

In general an arbitrary molecular absorption line exhibits a naturally broadened Lorentzian line shape which is further broadened by thermal motion and collisions between molecules. The Voigt function, which is usually calculated through convolution of Gaussian and Lorentzian profiles, is the function used to calculate the absorption coefficient line shape. At tropospheric densities, the lineshape is predominantly collisionally broadened (Lorentzian), however for accuracy, the Voigt function is adopted here. In the 1140 nm region, H_2O is the only major absorber and the Beer-Lambert law can be solved for the absorption coefficient which is the product of the linestrength and line shape function,

$$\sum_{i=1}^{N} S_i f(\nu,\nu_i,\gamma_i^p,\gamma_i^T) = \frac{\ln[T(\nu)]}{\rho x} \tag{2}$$

Expressed in this way, the absorption coefficient has all the model parameters on the left-hand side of the equation and all the measured parameters on the right hand side. The absorption coefficient can then be constructed from the parameters of the HITRAN database. For

computational simplicity, a closed-form approximation of the Voigt function, accurate to within 3%, was used [*Arnold et al., 1969*]:

$$f = f_0\left\{(1-r)\exp\left(-2.772z^2\right)+\frac{r}{1+4z^2}+0.016r(1-r)\left[\exp\left(-0.4z^{2.25}\right)-\frac{10}{10+z^{2.25}}\right]\right\} \quad (3)$$

where, r is the ratio of the pressure-broadened width and the Voigt width, γ_L/γ_V. The centerline value and parameter z are defined as:

$$f_0 = \left\{\frac{\gamma_V}{v_0^2}\left[1.065+0.447r+0.058r^2\right]\right\}^{-1} \quad (4)$$

$$z = \frac{v_0^2}{\gamma_V}\left(\frac{1}{v}-\frac{1}{v_0}\right) \quad (5)$$

The width of the Voigt profile is expressed in terms of the pressure-broadened width, γ_L, and the Doppler width, γ_G,

$$\gamma_V = \frac{\gamma_L}{2}+\sqrt{\left(\frac{\gamma_L}{2}\right)^2+\gamma_G^{\,2}} \quad (6)$$

The accuracy of the Voigt approximation was verified by using the function for an example water vapor absorption line and comparing the results with the same absorption line predicted through convolution of the Doppler and collisional components. A plot of this comparison is shown in figure 1 from which it is concluded that the approximation is of sufficient accuracy for this work.

In general, line strengths and line widths are temperature dependent. In this study the temperature and pressure was not controlled so the data were modeled according to laboratory conditions from which the line strengths and widths at the reference temperature were obtained. The spectroscopic water vapor parameters were extracted from HITRAN at the reference temperature (T_{REF} =296) and pressure (1 atm) and used to calculate the line strength and width for the laboratory conditions. The linestrength at any given temperature is given by

$$S(T)= S(T_{REF})\frac{Q(T_{REF})}{Q(T)}\frac{\exp(-hcE/kT)}{\exp(-hcE/kT_{REF})}\frac{[1-\exp(-hc\nu_0/kT)]}{[1-\exp(-hc\nu_0/kT_{REF})]} \quad (7)$$

where E is the lower state energy, and Q is the temperature dependent partition function. The symbols h, c, and k are the normal fundamental physical constants. The range of temperatures experienced in this study ranged from 296 to 298 K; therefore the assumption was made that the ratio of partition functions for two closely measured temperatures is unity. The validity of this assumption was tested using TIPS.FOR program included in the HITRAN 96 software suite (done at NASA Ames Research Center). The ratio of partition functions at 296 and 297 K was

found to be 1.005 which was significantly less than all other sources of error in the data analysis. Given the temperature and pressure, the pressure broadened line width is given by,

$$\gamma^{p}(T) = \left(\frac{T_{REF}}{T}\right)^{n} \left[\gamma^{*}_{air}(p - p_{w}) + \gamma^{*}_{self}(p)\right] \tag{8}$$

where p is the total air pressure whose value was obtained from the national weather service, n is the HITRAN temperature coefficient, and p_w is derived from independent temperature and relative humidity measurements. The * indicates that the value is for the reference temperature and pressure.

The HITRAN database contains many more parameters than we were able to measure, therefore the parameters were prioritized according to their importance under laboratory conditions. HITRAN parameters listed for water vapor include isotopic abundance, line position, linestrength, air-broadened half width, self broadened half width, lower state energy, line width temperature coefficient, line position pressure shift, quantum state indices, and error codes. Although the our experimental platform is capable of 0.001 cm^{-1} resolution, line position and pressure shifts were not accessible due to the restriction of scanning time, changing laboratory conditions, and laser shot variability. Therefore, we imposed restrictions on scan time (i.e., resolution) and made the assumption that line positions were sufficiently accurate to use for wavenumber calibration of the observed spectra. In regard to linewidths, the laboratory conditions produced lines that were predominantly widened by N_2 broadening (referred hereafter as air-broadening). Given that laboratory temperatures were near 296 K, our studies were insensitive to temperature coefficient errors. Furthermore, time constraints did not allow us to pursue temperature studies on water vapor lines, which would allow for investigations of temperature coefficient accuracy. Therefore, the parameters chosen for investigation here include linestrengths and air-broadened halfwidths.

III. Results and Discussion

A. Experimental Description

In this section we describe system details and report all experiments and results. The experimental platform was rearranged for some of the experiments; however, the basic configuration is shown in figure 2. The figure shows the most complex setup which was used for the water vapor spectroscopy experiments. For all work that was done in the 759-700 nm range, only the diode laser was used. The primary focus of the diode laser work was to explore various means of wavelength control and to test the capability of doing atmospheric measurements with the diode laser control system. The alexandrite laser was primarily used to access the 1140 nm band of water vapor.

1. Diode laser

The model 2010 tunable diode laser (Environmental Optical Sensors Inc. / Newport) was used for frequency locking experiments, O_2 rotational temperature measurements, and is the wavelength source for the alexandrite laser. The laser cavity is a piezo-tuned Littman-Metcalf external design and has a 100 kHz line-width specification. For atomic and molecular

spectroscopy experiements, the laser beam from the diode laser was split 90/10 with the stronger component beam optically coupled to a single mode fiber to be used for Fabry-Perot interferometry or, in the case of the atomic spectrscopy experiments, used as a pump beam for saturation. The weaker component was directed through an absorption cell (Rb, K, O_2) and sensed with a Thorlabs Si detector with rise time 1 ns and 0.8 mm^2 active area. Associated with the diode laser controller is the "lock box" servo control unit. The lock box uses the signal from the detector and provides a 400 Hz modulation with variable gain of an absorption feature peak when locked. The lock box also provides DC control of the laser wavelength range through application of an offset voltage on the piezo. Observation of the absorption features was attained with a 40-50 Hz, 7 Volt peak-to-peak modulation of the piezo. The absorption cells used in this work include the two atomic references, which are both 3" long by 1" diameter sealed Pyrex cells, and a variable path length open air White cell for oxygen measurements.

Tunable laser diode frequency-locking in the near-IR is important for atmospheric remote sensing since it provides precise spectral referencing and frequency stabilization [*Tetu et al., 1991, Zahn, 1996*] . The frequency references on which we focussed in this work includes ^{87}Rb D_2-line ($5S_{1/2} \leftrightarrow 5P_{3/2}$, 780 nm), ^{39}K D_1-line ($4P_{1/2} \leftrightarrow 4S_{1/2}$, 770 nm), O_2 A-band P-branch ($b^1\Sigma_g^+$ (v=0) $\leftarrow$ $X^3\Sigma_g^-$ (v=0), 767 nm). These references were chosen for investigation for several reasons. Firstly, the vapor pressure of rubidium at room temperature is sufficiently high to readily observe absorption. Secondly, potassium is important for remote sensing of thermosphere temperature, and finally, the P-branch of O_2 provides many spectral references for water vapor spectroscopy. With the exception of Rb, these references lie within operating range of the alexandrite laser. In the case of Rb, an appropriate output coupler for the alexandrite laser would allow operation at 780 nm.

In preparation for tropospheric lidar measurements of temperature and humidity, methods of diode laser frequency-control were investigated, for use with the alexandrite laser diode injection control. Among these investigations, the O_2 A-band rotational manifold was measured from which the P-branch rotational temperature was determined. In this experiment, the diode laser fiber coupler was removed to utilize the full strength of the beam and was propagated into a open air White cell which was comprised of two 12" f/8 gold coated spherical mirrors separated confocally by 1.63 meters. The laser beam was divided 50/50 at the output with one component fiber-coupled to a Burleigh wavemeter for independent wavelength measurement and monitoring of laser modal quality. The Burleigh instrument is accurate to ~0.1 nm. The other component was propagated into the White cell, which after 22 passes resulted in a total optical path length of 36 meters.

The rotational temperature was determined by performing a Boltzmann analysis of the measured transmittance of the ^{P}P-branch rotational lines. Applying the relationship between the Einstein *A* and *B* coefficients and the absorption coefficient [*Koechner, 1996*], the Beer-Lambert law takes a form which can be manipulated into a linear relationship where slope is the inverse of the rotational temperature and the intercept contains information about the total molecular concentration.

$$\ln\left(-\frac{\lambda_i \ln \tau_i}{f(\nu_i) S_i}\right) = \ln\left[\frac{hxKN_0}{Q}\right] - \frac{1}{T_{rot}}\left(\frac{hcF_i}{k}\right) \tag{9}$$

In the expression, τ_i is the peak transmittance of an *i*th absorption line, $f(\nu_i)$ is the line center value of the absorption line shape, N_0 is total molecular concentration, K represents the

relationship between the Einstein B coefficient for absorption and the linestrength S_i, Q is the partition function and F_i is the lower state energy. Linear regression of the measured O_2 peak transmittance data yielded a least-squares best fit of 300 K which was expected from room temperature measurements by the temperature sensors used in this work. In figure 3, the Boltzmann analysis for the O_2 A-band ^{P}P-branch is shown for the measurement of laboratory temperature. Under laboratory conditions, the O_2 molecule is well equilibrated thermally, and therefore its rotational temperature reflects the ambient laboratory temperature. In the data analysis, an upper bound of 4% error in measured transmittance was used for the error bars although the real measurement error was probably much smaller. The rotational lines measured for the plot included K=1 through 27. For the least temperature sensitive K=11 line, a 30°F change results in a 0.8% change in the datum whereas for the more temperature sensitive K=21 line a 30°F change results in a 2% change in the datum. From this measurement we conclude that spectroscopic observation and atmospheric temperature measurement using the O_2 rotational manifold can easily be accomplished.

Rubidium vapor has an appreciable room temperature vapor pressure and hence a usable resonance absorption cross section. Its resonance lines occur near the O_2 A-band and the potassium resonance lines, so Rb frequency locking is easily achieved with our experimental platform. Unlike the collisionally broadened lines of O_2, the spectral lines are only Doppler broadened and therefore have a more narrow profile. In the Doppler limited spectrum, the Rb fine structure lines have widths of the order of 600 MHz. However, through the use of saturation techniques, the hyperfine structure in the Rb manifold can be isolated, allowing for much narrower absorption features for frequency locking. For example, the $5S_{1/2}$, F=2$\leftrightarrow$$5P_{3/2}$, F=3 hyperfine component has a width of 35 MHz [*Tetu et al, 1991*]. Frequency locking to this feature would result in a diode laser frequency-locked at about the 5-10 MHz level. We observed a saturated spectrum to lay the ground work for a more precisely locked laser but did not perform the locking experiments due to time constraints. Figure 4 shows the Doppler-limited and saturated spectrum of Rb. In figure 5 Fabry-Perot images are shown for the diode laser unlocked and locked to the strongest feature of the Doppler limited Rb D_2-line. For the unlocked laser, it is noted that this etalon has an instrumental line shape much wider that the laser line width; therefore, the unlocked laser provides a convenient means for measurement of the instrument resolution of the etalon. In this example the etalon signature is commensurate with the instrument resolution (20 MHz). For the locked laser, the lock gain has been set to maximum to illustrate the upper limit of the lock bandwidth. The lock bandwidth is about 200 MHz. For actual locked laser operation the gain would be decreased to produce a laser locked to about 30-50 MHz.

Potassium occurs in the atmosphere naturally because of meteoric dust. The resonance lines occur near the O_2 A-band at 770 nm , and the fine structure exhibits a high degree of spectral blending. The vapor pressure of potassium at room temperature is not sufficiently high for resonance absorption spectroscopy, so a temperature controlled heating apparatus was engineered for the potassium experiments. At 180°F sufficient absorption occurred, and the associated fluorescence was bright enough to be observed with a CCD camera and an IR viewer. Frequency lock stability was investigated in the potassium channel since stability of the system is considered to be crucial in the remote sensing of potassium derived temperatures of the mesosphere. In one experiment, the locked diode laser was monitored over a four hour period with a lock gain set to produce a line width of 180 MHz. The wavelength drifts observed during the period were no more than several pixels in the CCD image of the Fabry-Perot interferometry.

In this case, a one pixel change in radius is equivalent to a $5x10^{-7}$ nm change in wavelength. Therefore the stability of the locked diode laser is such that the laser drift over the course of several hours is not expected to exceed 10^{-6} nm.

2. Alexandrite Laser

Details of the alexandrite laser cavity have been described elsewhere [*Walling et al., 1980; Guerra, 1993; von Zahn et al., 1996*] and only salient details will be covered here. The alexandrite laser was operated at a pulse repetition frequency of 20 Hz and provided the source for the water vapor spectroscopy measurements. The laser, when Q-switched, exhibits a 100 mJ pulse with a TEM_{00} beam of diameter 2-3 mm. Temporally, the laser exhibited a nearly Gaussian fundamental pulse of about 180 ns in duration. The time resolved pulse from the fundamental output (Thorlabs 1 ns Si detector) and first Stokes Raman shifted output (Thorlabs 5 ns InGaAs detector) were Fourier transformed for laser lineshape characterization and bandwidth measurement. Figure 6 shows these results. From the figure it was deduced that the line width in the fundamental is roughly 10 MHz and in the infrared it is roughly 20 MHz with the largest sidelobe features 1/7 that of the main peak. Given that the water vapor features of interest are typically not less than 1.5 GHz, this source has sufficiently narrow bandwidth for near-IR water vapor spectroscopy.

Wavelength tunability was accomplished through the fiber-coupling between the alexandrite cavity and the diode laser (commonly referred to as seeding or injection). Proper alignment and optimization of the seed laser injection produces single mode operation of the alexandrite at the desired wavelength. When optimized, the laser wavelength can be modulated to span 4 cm^{-1} while producing good single mode shots and minimal degradation of power.

The spectral purity of the alexandrite output pulses was monitored during data acquisition with a temperature stabilized Fabry-Perot etalon whose images were captured with a Cohu 4915 CCD camera and Spiricon laser beam profiler. The etalon has a plate separation of 15 cm and has a free spectral range of 1 GHz with a resolution of 20 MHz. In figures 7, CCD images of the Fabry-Perot interferometry are shown of the alexandrite output at 770 nm. With 100 kHz laser line width, the diode laser has much smaller bandwidth than the 20 MHz resolution of the etalon. Therefore Fabry-Perot analysis is a good measure of instrumental characterization of the etalon. The alexandrite operational stability was also continuously monitored during data acquisition through photodiode (Thorlabs) and pyroelectric detection (Ophir) of the output pulses, which provided time resolved shot profiles and power levels.

3. Frequency Conversion

The alexandrite laser beam was Raman shifted into the infrared (first Stokes) with a 1 meter 350 psi hydrogen Raman cell made by Light Age, Inc. Optimization of conversion was desired to minimize shot-to-shot variability and pulse irregularity. This was accomplished in two ways: First, Raman conversion efficiency experiments were performed in an effort to better understand stimulated Raman scattering (SRS) processes and optimize the conversion to the 1140 nm channel. Second, the technique of external beam expansion before insertion into the Raman cell was employed to enhance conversion. The external beam expander consists of a –10 cm F.L. lens and a +15 cm lens arranged so that their separation could be adjusted to maximize the resulting conversion efficiency.

Raman conversion was measured for 2nd order and 1st order anti-Stokes and 1st order Stokes channels for pressures ranging from 125 to 500 p.s.i. Expected conversion efficiencies were of the order of 45% [*Chu, 1991*] however observed efficiencies were found to be on the order 1% for the 1st order Stokes and significantly and inexplicably less for the others. One possible explanation for this result may be due to beam wandering. The measurements were made using fast detectors which by their nature have small active areas (less than 1 mm^2) to achieve their fast response times (1 and 5 ns for Si and InGaAs respectively). Observed beam diameters of the Raman beams were roughly 8 mm in diameter for both anti-Stokes orders and 2 mm for the Stokes order. These geometrical factors were included when the data were analyzed; however the measurements were made in an averaging fashion. The alexandrite laser rods are known to exhibit positive thermal lensing. Although negative lenses are incorporated in the cavity design to stabilize the cavity, beam wandering becomes more significant at longer distances, especially when sensing with small area detectors. Figure 8 shows the observed average Raman pulse energies. The important conclusion made here is that in the infrared (1st order Stokes), a Raman cell pressure of 350 p.s.i. is the optimal Raman cell pressure for operation.

The alexandrite laser is capable of lasing across a wavelength range from 701 to 818 nm [*Guerra, 1993*]. Raman conversion and frequency doubling extend this capability from the UV to the Far-Infrared. Consequently, wavelength stabilization becomes a crucial issue to accessing the many channels of interest to the atmospheric remote sensing community. In this work we explored wavelength control through the use of K, Rb, and O_2 absorption lines, however, as of 1997, commercially available atomic vapor cells included iodine, cesium, rubidium, potassium, sodium, and lithium. These elements have absorption features of well-known position that occur within the operational envelope of the alexandrite laser (720-800 nm). The wavelengths that would be generated for hydrogen Raman conversion and frequency doubling are shown in figure 9. The figure illustrates the many channels that can be generated; however the plot is not exhaustive. For sodium and lithium there is an absence of usable lines in the 720-800 nm range, however, for the other elements and O_2, there exists over 103 usable references for wavelength control. For hydrogen Raman conversion alone (4th, 3rd, 2nd, 1st anti-Stokes and 1st, 2nd, and 3rd Stokes channels), 824 channels can be generated and if combined with frequency doubling, over 2400 channels can be generated. Other gases for Raman cells are available as well such as nitrogen, deuterium, and methane.

B. Water Vapor Measurements

The atmospheric transmittance spectrum was measured using pyroelctric detection of the filtered First Stokes laser light with a Laser Precision Corporation Rj-7200 Energy Ratiometer. As shown in figure 2, the Raman shifted laser pulses were split into two beams in which one component was captured by detector A before insertion of the other component into the White cell. Detector B captured the second component at the output of the white cell. The instrument was later calibrated against a known transmittance and verified through independent measurement with second detection system.

The White cells used in this work consist of two 6" f/7 gold-coated mirrors with a 1.8 meter separation (O_2) and two 12" f/8 gold-coated mirrors with a 2.3 meter separation (H_2O). For the alexandrite laser, the beam was reflected at the Raman cell output with an uncoated plate beam splitter to avoid exceeding the recommended energy density threshold on the detectors and was spectrally filtered with a 1000 nm cutoff long pass filter. The beam was then spatially filtered with a variable iris to produce a clean single beam which was then directed into the f/8 White

cell with a small 1"x2" gold coated mirror. After 53.5 meters of traversal, the beam was extracted with a small 0.5" corner cube prism. The beam was spatially filtered again at the prism with 2 mm aperture. The White cell path length was measured by time-of-flight measurement with two InGaAs detectors in the infrared. Figure 10 shows the time of flight measurement, which consists of the laser pulse measurement at the input to the white cell and the laser pulse at the output.

Spectral scanning of the spectrum was done *via* DC biasing of the diode laser piezo driven cavity in 0.05 cm^{-1} intervals. Each scan took approximately 45 minutes to acquire, covering roughly 4 cm^{-1}, and five measurements were recorded at each wavenumber interval to obtain a mean and standard deviation for each datum and associated error bar. In addition to the spectroscopic measurement, the ambient temperature and relative humidity were simultaneously measured with three different sensors whose values were subsequently used to derive temperature and water vapor concentrations. The sensors were manufactured by Hanna (HI 8064 hygrometer), Vaisala (HM141 humidity and temperature sensor), and Mannix (LAM880D temperature and humidity sensor). These instruments were later compared against an identical Vaisala model which is used for calibration at NOAA. The temperature and relative humidity records is shown are figures 11.

15 lines of the $2\nu+\delta$ water vapor band in the wavenumber range 8865-8915 cm^{-1} were observed for measurement of their line strengths and air-broadened half widths. The data were taken on UT days 277-284, 2000. Figure 12 shows the water vapor spectrum in this region and the associated O_2 A-band whose rotational lines provided spectral referencing before Raman shifting. In the figure, the O_2 A-band wavenumber axis has been Raman-shifted to illustrate the relationship between the alexandrite fundamental frequency and the associated Raman conversion of that frequency. The first group of water vapor lines that were investigated is found near 8885 cm^{-1} or, in the fundamental, near the $^{P}P21$ line of O_2. The water vapor lines are identified as the (404-303), (321-211), (321-220), and (414-313) transitions. These lines were measured multiple times over multiple days and different path lengths to better understand the performance of the laser and atmospheric conditions in the lab. Figure 13 shows a plot of the these lines measured in transmittance for three different path lengths and the results of the modeling. As a function of path length, HITRAN line strengths and line widths consistently produced line profiles that underpredicted observations.

Laser operational stability was not repeatable every day. Alexandrite cavity optimization, diode injection alignment, birefringent tuner adjustment, and white cell alignment had to repeated every time a new part of the spectrum was investigated. In some scans, for example, diode mode hopping was problematic until birefringent tuner adjustment was accomplished to produce a consistent mode hop free scan. Each part of the spectrum investigated was done multiple times to get the most consistent set of results. This process was repeated for each line or set of lines. For the final set of data, only the best scans were chosen for final analysis.

C. Comparisons to HITRAN-2000

The transmittance spectrum was first converted to the absorption coefficient through implementation of equation 2. Observed spectra containing multiple lines were wavenumber calibrated using the HITRAN-2000 water vapor line positions in a linear sense using two lines. In those cases where only a single line was measured, the average calibration from all multiple line measurements was used. Background correction was accomplished by fitting off-line regions

in the data to the predicted values by a trial-and-error basis. Best fits between model and data were done for each individual line to avoid background error contaminating the far line fits. During this trial and error process, the sum of the square of the differences between the model and data was calculated to aid in the minimization of the least squares values. Given the complexity of the Voigt approximation used in the work, derivation of analytical relationships of the least squares fit was not possible.

The atmospheric transmittance data were acquired as a data set of five measurements for each wavenumber interval. The choice of this number was based on the recommendation that at least five measurements should be used when calculating a mean and associated standard deviation [*Taylor, 1982*]. However more measurements would have lengthened the time of the scan thereby increasing the susceptibility of the data to laser operational variability. Once the mean transmittance was obtained, the absorption coefficient was calculated from the measured path length and measured water vapor concentration. The line strength at the reference temperature, (T_{REF}=296K), was calculated using the modeled line shape parameters and then corrected for temperature:

$$S_{REF} = -\frac{A}{f_0 n_W x}\ln\left(\frac{1}{5}\sum_{i=1}^{5}\tau_i\right)\frac{\exp\left(-hcF''/kT_{REF}\right)\left[1-\exp\left(-hc\nu_0/kT_{REF}\right)\right]}{\exp\left(-hcF''/kT\right)\left[1-\exp\left(-hc\nu_0/kT\right)\right]} \tag{10}$$

Although it was shown earlier that the widths are predominantly Lorentzian, the measured widths are treated as Voigt widths. Given the measured temperature, the Doppler width was calculated and used with the measured Voigt width to calculate the total pressure-broadened width:

$$\gamma_P = \frac{\gamma_V^2 - \gamma_G^2}{\gamma_V} \tag{11}$$

Once the total pressure broadened half width was obtained, the air-broadened half width was calculated using the measured total and partial water vapor concentrations and the HITRAN tabulations for temperature coefficient and self-broadened halfwidth.

$$\gamma_{air} = \left(\frac{1}{p-p_W}\right)\left[\left(\frac{T}{T_{REF}}\right)^n(\gamma_P) - (p_W)(\gamma_{SELF})\right] \tag{12}$$

The measured widths and peaks of the absorption features formed the central data pair from which the air-broadened halfwidths and line strengths were determined. Table 1 lists the linestrengths from HITRAN-2000, recent theoretical predictions from Nasa-Ames Research Center and the observed linestrengths, and Table 2 lists the air-broadened halfwidths from HITRAN-2000 and the observed widths. We find that the observed linestrengths compared to HITRAN-2000 are a factor of 1.28 (±13%) larger on average and the observed widths are larger by a factor of 1.13 (±21%). The error propagation analysis is described below. The results of this data analysis are shown graphically in figures 14 through 17. In figure 14, the observed linestrengths are compared to HITRAN-2000 and the plot suggests that the current HITRAN

tabulations are systematically underestimated. On average, the observed widths in figure 15 are larger than the HITRAN entries however, the observed scatter in the data is more pronounced. The measured strengths and widths covered a range of lower state energies from 80 cm^{-1} to 327 cm^{-1} . The dependence of the strengths and widths on lower state energy was also investigated. In figures 16 and 17, the data are ratioed to HITRAN and plotted as functions of lower state energy. The plots suggest no lower state energy dependence in the deviation of the results with HITRAN. In summary, these results are consistent with growing evidence that the HITRAN compilations for the near-IR lines of H_2O are in need of critical review and further measurements.

D. Error Analysis

Error bars in the data were calculated from error propagation from laser fluctuations, relative humidity and temperature measurement error, path length uncertainty, Voigt approximation error, and calibration uncertainties. Not included in the error analysis are contributions from background fluctuations that were found to be non-systematic and non-repeatable but probably only contributed to uncertainties at the 5% level. The error propagation equations are described here.

The line strength error bar was calculated from the standard deviation of the five measurements of atmospheric transmittance. This represented the shot-to-shot variability of the laser. Error propagation of the standard deviation results in the total error for the line strength:

$$\delta S = \left(\frac{A}{f_0}\right)\delta q \tag{13}$$

The uncertainty in the air-broadened half-width measurement was calculated for the uncertainties in the Voigt and Gaussian components. The total uncertainty is usually calculated as the square root of the sum of squares of the uncertainties, however, in this analysis, the ordinary sum of individual was used to determine the upper limit of the error bar:

$$\delta\gamma_{air} \le \left|\frac{\partial\gamma_{air}}{\partial\gamma_V}\right|\delta\gamma_V + \left|\frac{\partial\gamma_{air}}{\partial\gamma_G}\right|\delta\gamma_G \tag{14}$$

For the Gaussian component, the error was assumed to be dominated by the uncertainty in the measured temperature. Using the Doppler profile, the propagated temperature uncertainty gives the error bar for the Gaussian component:

$$\delta\gamma_G = \left(\frac{\nu_0 k \ln 2}{mc}\right)\frac{\delta T}{\sqrt{2\ln 2 kT/m}} \tag{15}$$

For the Voigt component, the uncertainty was calculated from the expression for the center value of the Voigt function (eq. 3). Since the width was measured at the half maximum of value of the absorption profile, the error was assumed to be dominated by the uncertainty in the measured peak. The propagated peak error then gives the error bar in the Voigt component:

$$\delta\gamma_V = \frac{10^7 \delta f_0}{\lambda_0^2 4a}\left|1 - \frac{\beta - f_0^{-1}}{\sqrt{\left(\beta - f_0^{-1}\right)^2 - 4ac}}\right| \tag{16}$$

Using these errors in the expression for the uncertainty in the air-broadened half-width gives the total error bar:

$$\partial\gamma_{air} = \left(\frac{1}{p - p_W}\right)\left(\frac{T}{T_{REF}}\right)^n\left[\left(1 + \frac{\gamma_G^2}{\gamma_V^2}\right)\delta\gamma_V + \frac{2\gamma_G}{\gamma_V}\delta\gamma_G\right] \tag{17}$$

Table 1. Comparison of measured linestrengths to Hitran-2000 and recent theoretical work from NASA Ames Research Center.

Line (cm^{-1})	Hitran2k	Schwenke	Present work	E" (cm^{-1})
8866.1671	1.076e-21	1.087e-21	1.46e-21 (15%)	79.496
8877.2598	5.371e-23	7.483e-23	7.46e-23 (26%)	136.762
8879.1198	5.371e-22	7.222e-22	6.33e-22 (9%)	134.902
8882.8726	3.761e-22	5.222e-22	4.77e-22 (10%)	142.279
8884.0110	1.740e-22	2.407e-22	2.09e-22 (7%)	136.164
8884.4988	2.941e-22	4.220e-22	3.81e-21 (6%)	95.176
8885.5740	1.153e-21	1.651e-21	1.47e-21 (7%)	136.762
8887.7878	5.772e-23	5.903e-23	8.62e-23 (26%)	173.365
8898.1943	9.453e-22	1.330e-21	1.14e-21 (9%)	224.838
8899.1304	2.226e-22	3.021e-22	2.89e-22 (11%)	206.301
8899.6936	3.208e-22	4.509e-22	4.25e-22 (10%)	222.052
8906.3510	8.657e-22	1.272e-21	1.04e-21 (10%)	173.365
8907.9040	8.595e-23	1.181e-22	1.15e-22 (21%)	285.219
8912.2568	2.448e-22	3.259e-22	2.64e-22 (13%)	326.625
8912.9834	7.353e-22	9.857e-22	9.12e-22 (10%)	325.348

Table 2. Comparison of measured air-broadened linewidths to Hitran-2000.

Line (cm^{-1})	Hitran2k	Present work	E" (cm^{-1})
8866.1671	0.0973	0.12 (25%)	79.496
8877.2598	0.0919	0.097 (44%)	136.762
8879.1198	0.0937	0.12 (15%)	134.902
8882.8726	0.0908	0.10 (17%)	142.279
8884.0110	0.0914	0.084 (12%)	136.164
8884.4988	0.0972	0.095 (10%)	95.176
8885.5740	0.0912	0.15 (11%)	136.762
8887.7878	0.0975	0.12 (43%)	173.365
8898.1943	0.0812	0.092 (15%)	224.838
8899.1304	0.0917	0.090 (19%)	206.301
8899.6936	0.0837	0.094 (16%)	222.052
8906.3510	0.0922	0.096 (16%)	173.365
8907.9040	0.0849	0.096 (34%)	285.219
8912.2568	0.0778	0.075 (22%)	326.625
8912.9834	0.0750	0.083 (17%)	325.348

IV. Conclusions

We have succeeded in the development of a narrow line, broadly tunable alexandrite based laser transmitter suitable for DIAL measurements of water vapor and temperature in the near-IR. The laser has been optimized for higher pulse energy, higher stability operation, and a nearly pure TEM_{00} mode. The laser is seeded with a tunable diode laser whose wavelength can be modulated for high resolution scanning to 0.001 cm^{-1}. The addition of frequency locking instrumentation and a potassium vapor cell has resulted in a platform that can now be frequency stabilized for mesospheric temperature profiling.

Diode laser:	
Wavelength	765 nm
Bandwidth	15 nm
Laser line width	100kHz
Alexandrite laser:	
Fundamental tuning range	700-818 nm
Beam mode	TEM_{00}
Beam diameter	~3 mm
Pulse duration	180 ns
Pulse energy	100 mJ
Pulse repetition frequency	20 Hz
Fundamental laser linewidth	10 MHz
1^{st} Stokes line width	20 MHz

The first application of this development as been to make new measurements of selected lines 1140 nm band of H_2O. The need for spectroscopic improvements of the HITRAN database, particularly in the spectral region just beyond 1 micron, has been established in the literature. There is now a well recognized consensus for the improvement near IR water vapor parameters, particularly important for DIAL systems under development in the US and elsewhere. Lidar profiling of atmospheric water vapor must be done with DIAL in the near-IR in order to work in daylight and over a wide range of humidities.

In this work, high resolution scans for 15 water vapor lines occurring in the range 8865-8915 cm^{-1} were used for measurement of line strengths and air-broadened half widths. These results suggest that the lines are stronger and wider than shown in the HITRAN-2000 database. We also developed our own model, based on the current HITRAN database, for predicting the atmospheric transmittance spectrum. The development of this code enabled us to compare our measurements directly with HITRAN for validation.

Additionally, the diode laser, primarily used for seed injection of the alexandrite, was also used for spectroscopic measurements of rubidium, potassium, and molecular oxygen absorption lines. These experiments included investigation of frequency locking techniques that will be used in future remote sensing of temperature and humidity. Given the high-resolution capability of the system, the role of these atomic and molecular absorption features provided accurate spectral references that were crucial for the water vapor spectroscopy. Additionally, we tabulated all frequency standards available for the fundamental operating range of the alexandrite to map out the full capability of the system.

The system is currently configured with an output coupler which allows the water vapor spectrum to be readily accessed from 8825-8925 cm^{-1}. With the appropriate output coupler, the rubidium frequency standard would extend the operational capability to 8660 cm^{-1}. In this work, we used H_2 for Raman conversion. Similar applications and studies of the H_2O band region near 940 nm can be carried out through Raman conversion in D_2. Accurate parameters for the spectral lines of water vapor are essential for the continued development and validation water vapor lidar systems. The capability for atmospheric temperature profiling will also result from this R&D program.

References

Arking, A., Bringing climate models into agreement with observations of atmospheric absorption, *J. Climate*, 12, 1589 – 600, 1999.

Arnold, J.O., E.E. Whiting, and G.C. Lyle, Line by line calculations of spectra from diatomic molecules and atoms assuming a voigt line profile, *J. Quant. Spectrosc. Radiat. Transfer, 9,* 775-798, 1969.

Belmiloud, D., R. Schermaul, K.M. Smith, N.F. Zobov, J.W. Brault, R.C.M. Learner, D.A. Newnham, and J. Tennyson, New studies of the visible and near-infrared absorption by water vapour and some problems with the HITRAN database, *Geophys. Res. Letters, 27, No. 22,* 3703 – 3706, November 15, 2000.

Chevillard, J.-P., J.-Y. Mandin, J.-M. Flaud, and C. Camy-Peret, *Can. J. Phys.*, Vol. 67, pp. 1065-1084. 1989.

Chu, Z., Research on stimulated raman scattering with applications to atmospheric lidar, Ph.D. Thesis, University of Maryland, 1991.

Chu, Z, T.D. Wilkerson, and U. N. Singh, Water-vapor absorption line measurements in the 940-nm band by using a Raman-shifted dye laser, *Appl. Optics*, Vol. 32, No. 6, 20 Feb. 1993.

Espy, P.J. and M. R. Hammond, Atmospheric transmission coefficients for hydroxyl rotational lines used in rotational temperature determinations, *J. Quant. Spectrosc. Radiat. Transfer 54, No. 5,* 879-889, 1995.

Gamache, R.R., and R.W. Davies, Theoretical calculations of N2-broadened halfwidths of H2O using quantum fourier transform theory, *App. Optics*, Vol. 22, No. 24, p. 4013-4019, 1983.

Gamache, R.R., and L.S. Rothman, Temperature dependence of N2-broadened halfwidths of water vapor: the pure rotation and ν2 bands, *J. Molec. Spectrosc.*, Vol. 128, p 360-369, 1988.

Giver L.P., C. Chackerian Jr., and P. Varanasi, Visible and near-infrared $H_2{}^{16}O$ line intensity corrections for HITRAN-96, , *J. Quant. Spectrosc. Radiat. Transfer*, 66, 101-105, 2000.

Giver, L.P., B. Gentry, G. Schwemmer, and T.D. Wilkerson, Water absorption lines , 931-961 nm: selected intensities, N2-collision-broadening coefficients, self-broadening coefficients, and pressure shifts in air, *J. Quant. Spectrosc. Radiat. Transfer*, Vol. 27, No. 4, pp. 423-436, 1982.

Guerra, D.V., Stimulated raman scattering in molecular hydrogen pumped by a tunable alexandrite laser, Ph.D. Thesis, The American University, Washington D.C., 1993.

Gutman W.M., W.A. Peterson, B.K. Matise, J.L. Manning, and R.E. Soulon, Atmospheric transmission spectroscopy using the sun as the source, *Appl. Optics*, Vol. 29, No. 22, August 1, 1990.

Koechner W., *Solid-State Laser Engineering*, Springer,1996.

Lynas-Gray, A.E., S. Miller, J. Tennyson, Infrared transition probabilities for water: a comparison of ab initio and fitted dipole moment surfaces, *J. Molec. Spectrosc.*, Vol. 169, pp 458-467, 1995.

Mandin, J.-Y., J.-P. Chevillard, J.-M. Flaud, and C. Camy-Peyret, H_2O-16 – line positions and intensities between 8000-9500 cm^{-1}. The 2nd hexad of interacting vibrational states [(050), (130), (031), (210), (111), (012)], *Can. J. Phys. 66*, 997-1011, 1988.

Measures, R.M., Laser remote sensing, Krieger Publishing Co., reprint edition, 1992.

Partridge, H. and D.W. Schwenke, The determination of an accurate iosotope dependent potential energy surface for water from extensive ab initio calculations and experimental data, *J. Chem. Phys.*, Vol. 106, No. 11, 15 March 1997.

Rothman L.S., C.P. Rinsland, A. Goldman, S.T. Massie, D.P. Edwards, J.-M. Flaud, A. Perrin, C. Camy-Peyret, V. Dana, J.-Y. Mandin, J.Schroeder, A. McCann, R.R. Gamache, R. B. Wattson, K. Yoshino, K.V. Chance, K.W. Jucks, L. R. Brown, V. Nemtchinov, and P. Varanasi, The HITRAN molecular spectroscopic database and HAWKS (HITRAN Atmospheric Workstation): 1996 edition, *J. Quant. Spectrosc. Radiat. Transfer, 60,* 665-710, 1998.

Swensson, J.W., W.S. Benedict, L. Delbouille, and G. Roland, The solar spectrum from λ 7498 to λ 12016, Institut d'Astrophysique de l'Universté de Liège, Special Vol. 5, 1970.

Taylor, J.R., An introduction to error analysis: the study of uncertainties in physical measurements, p. 87, University Science Books, Oxford University Press, 1982.

Tetu, M., N. Cyr, B. V. Villeneuve, S. Theriault, M. Breton, and P. Tremblay, Toward the realization of a wavelength standard at 780 nm based on a laser diode frequency locked to rubidium vapor, *IEEE transactions on instrumentation and measurement*, Vol. 40, No. 2, april 1991.

Tepley, C. and M. Sulzer, *Arecibo Observatory Newsletter*, No. 30., August 2000.

von Zahn, U., and J. Hoffner, Mesopause temperature profiling by potassium lidar, *Geophys. Res. Let.*, Vol. 23, No. 2, p. 141-144, Jan. 15, 1996.

Walling, J.C., O.G. Peterson, H.P. Jenssen, R.C. Morris, E.W. O'Dell, Tunable alexandrite lasers, *IEEE Journal of Quantum Electronics*, Vol. 16, pp 1302-1315, 1980.

Wulfmayer, V., J. Bösenberg, S. Lehmann, C. Senff, and St. Schmitz, Injection-seeded alexandrite ring laser: performance and application in a water-vapor differential absorption lidar, *Optics Lett.*, Vol. 20, pp. 638-640, 1995.

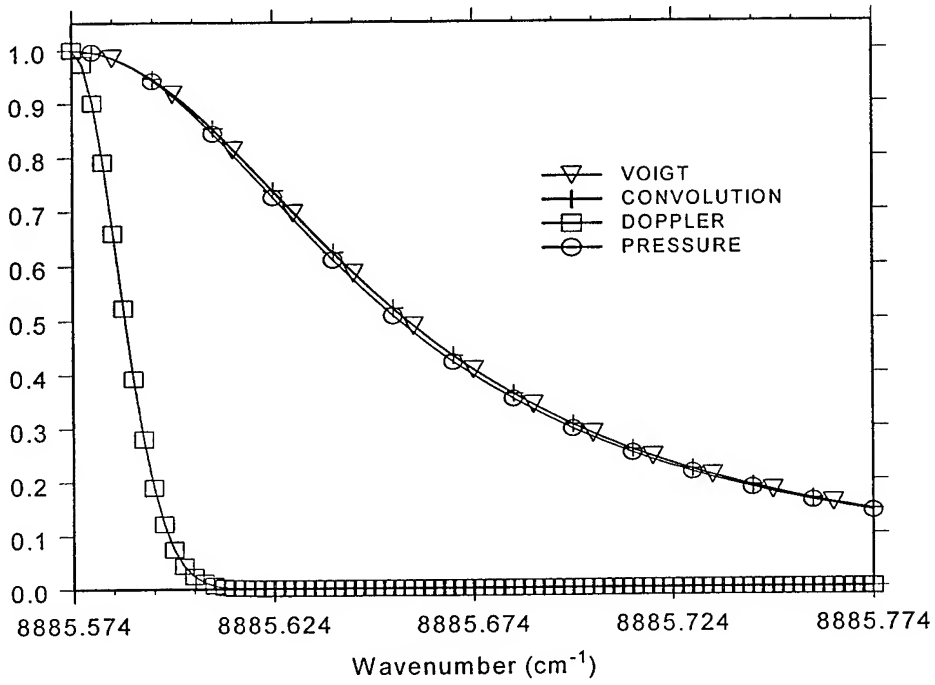

Figure 1. Voigt approximation model compared with direct convolution for the water vapor line near 8885.574 cm^{-1}.

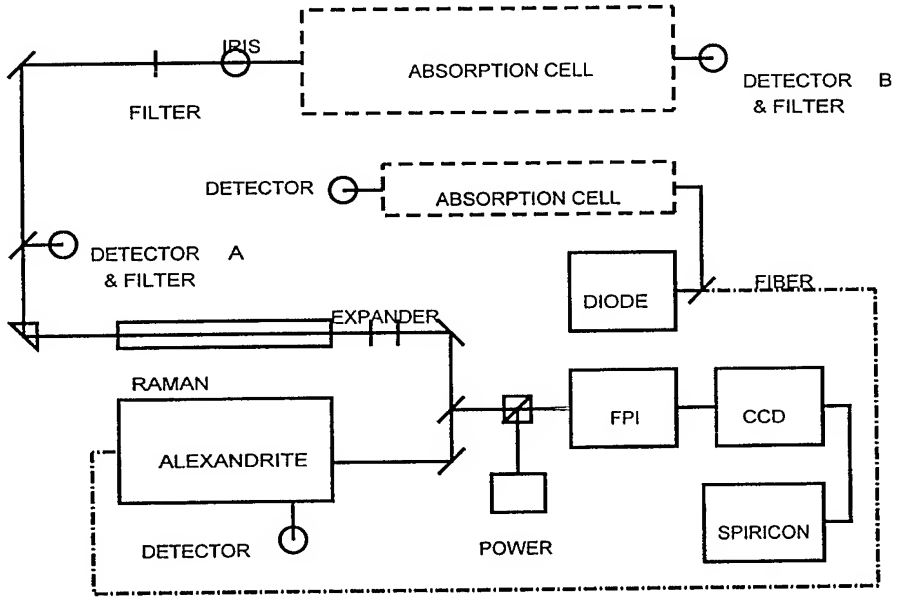

Figure 2. Experimental layout used for the measurement of water vapor absorption. In the figure, the first Stokes channel was used to access the 1140 nm water vapor band. All filters in the figure are 1000 nm longpass filters.

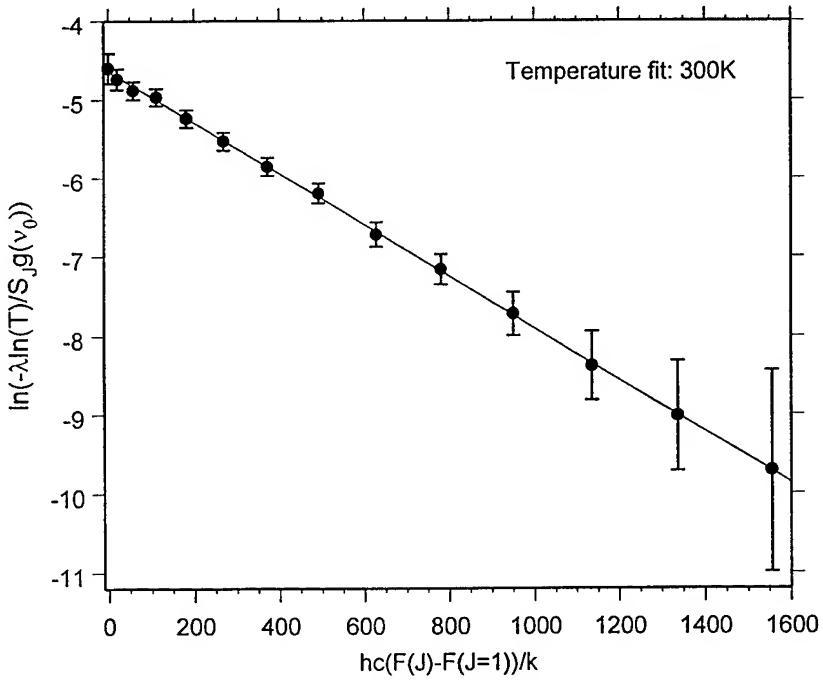

Figure 3. Oxygen A-band rotational temperature measurement. The error bars are based on 4% uncertainty in the transmittance measurement. Error propagation formulas were derived from the Beer-Lambert law of absorption. The temperature was determined from linear regression of the data.

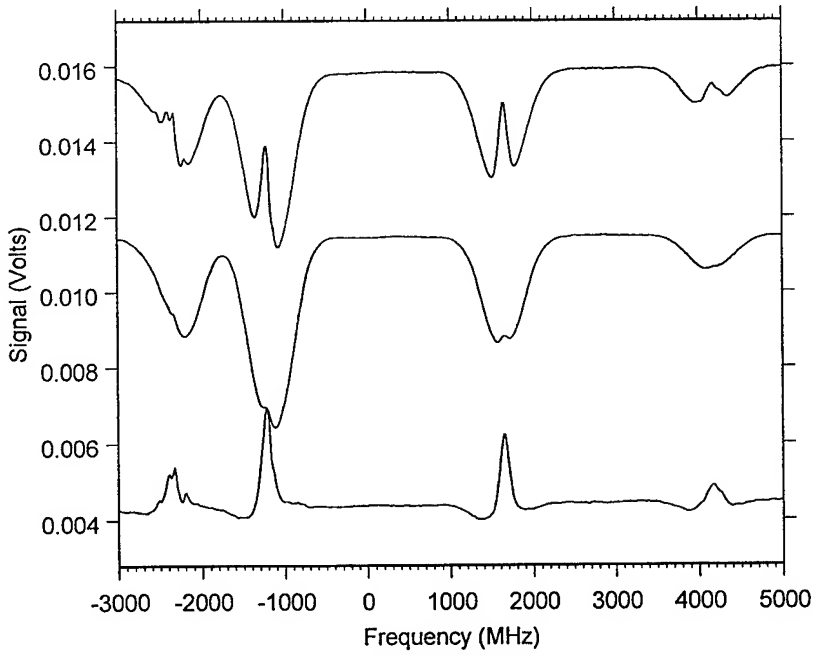

Figure 4. Saturated and unsaturated rubidium spectrum. The center frequency at 0 MHz corresponds to 780.03 nm. The wavelength axis was calibrated against the fine structure line positions.

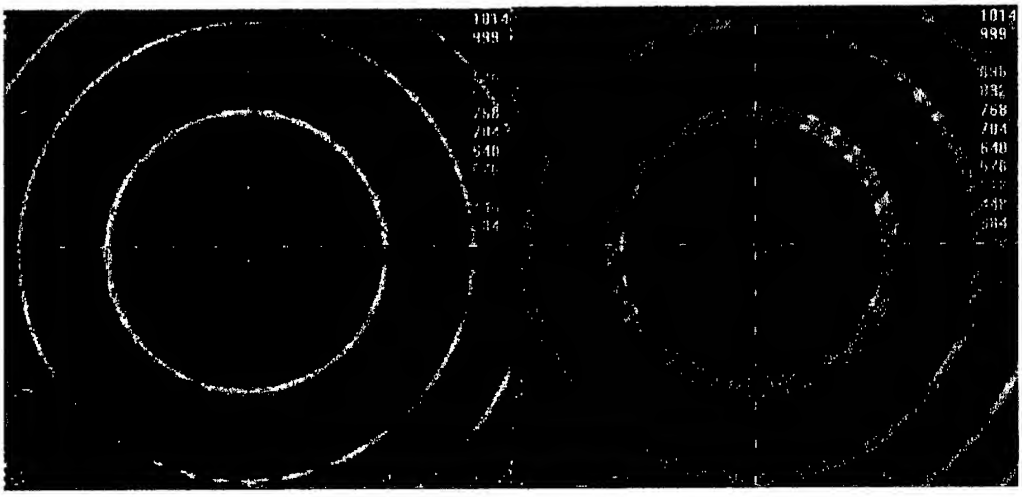

Figure 5. Fabry-Perot interferometry of 780.03 nm diode laser unlocked (Left) and frequency locked to the largest rubidium Doppler limited feature. The frequency lock gain was set at maximum to illustrate the upper bound lock bandwidth (~200 MHz).

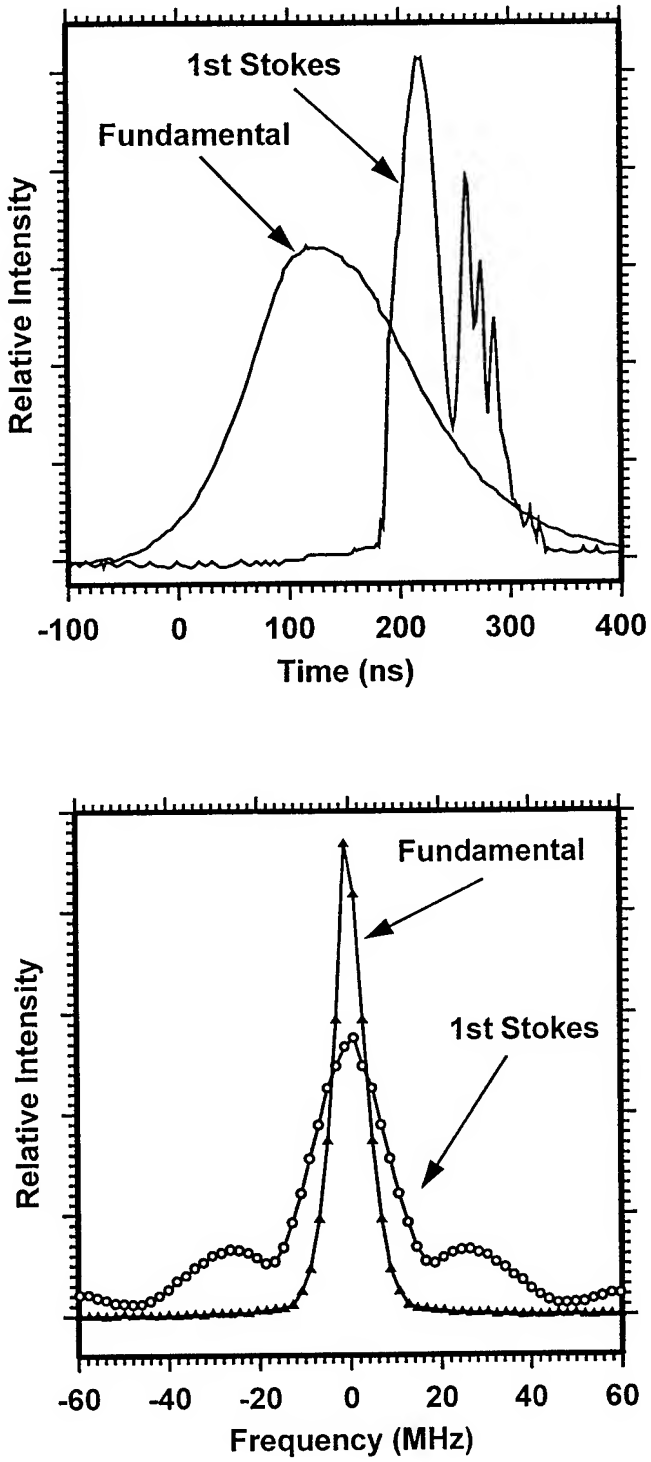

Figure 6. Fourier Analysis of the Alexandrite laser output. The fundamental output is near 770 nm with a nearly Gaussian 10 MHz linewidth. The First Stokes channel is near 1132 nm with a linewidth of roughly 20 MHz. The first sidelobe in the First Stokes channel is nearly 1/7 that of the main peak.

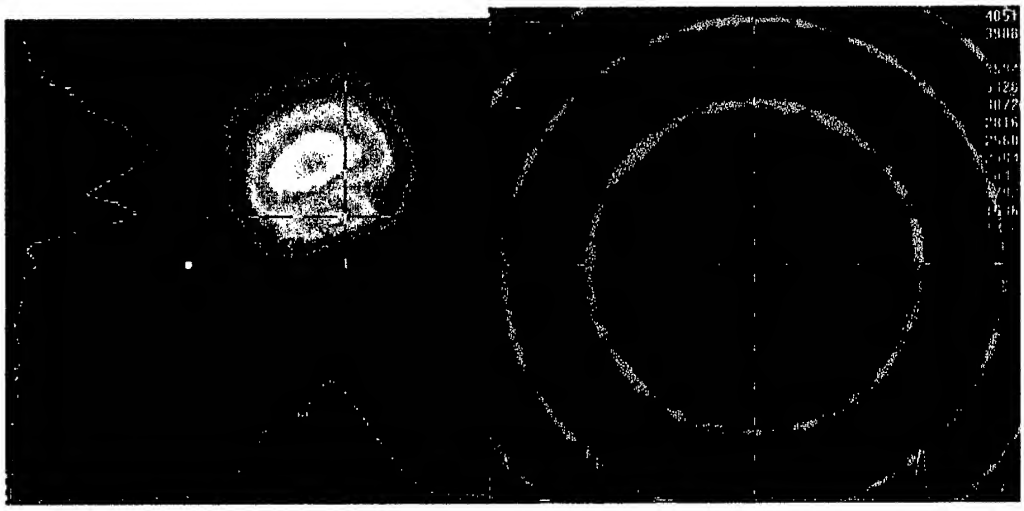

Figure 7. Alexandrite laser beam spatial profile and Fabry-Perot interferometry. The spatial beam profile is nearly TEM00 at least in one axis. The Fabry-Perot signature shows good single mode performance.

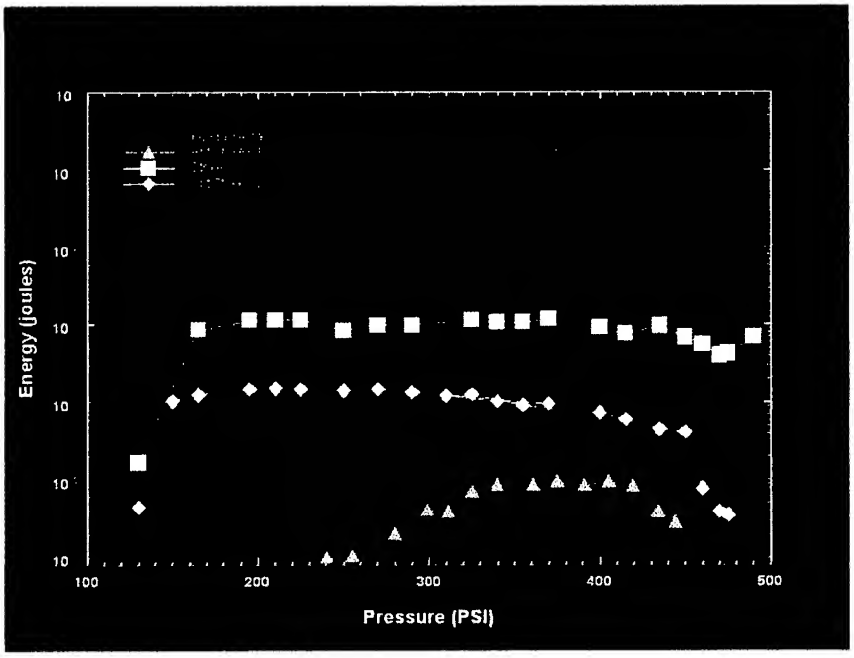

Figure 8. Raman conversion efficiency of the 1st Stokes and 1st and 2nd anti-Stokes output. The 1st stokes efficiency is on the order of 1% with a peak efficiency near 350 p.s.i.

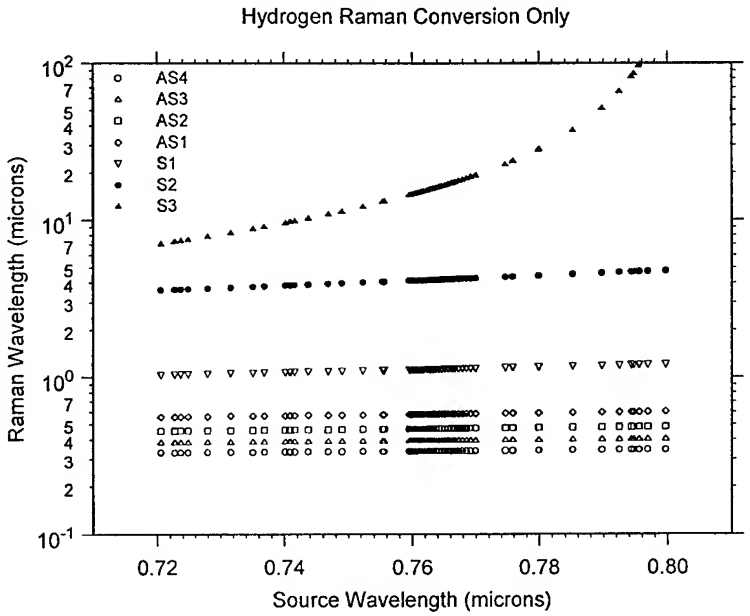

Figure 9. Hydrogen Raman channels generated from all tabulated atomic and O_2 absorption line wavelengths that occur within the operational envelope of the Alexandrite laser.

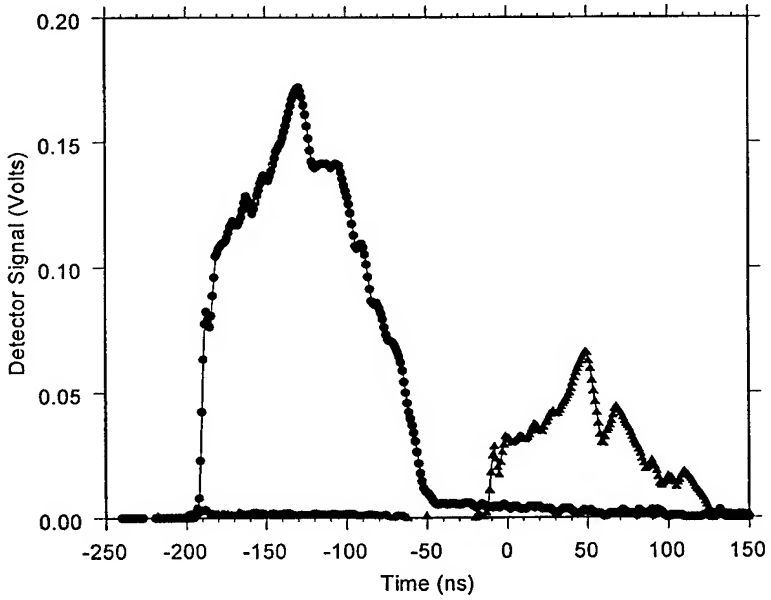

Figure 10. The total optical path length of the White cell configuration used for the water vapor measurements was determined by time of flight for the 1st Stokes channel. The laser beam was sensed with an InGaAs 5 ns rise time detector at the input to the White cell and again with a second detector at the output. Time differences measured between major peaks resulted in an average measured path length of 55 meters.

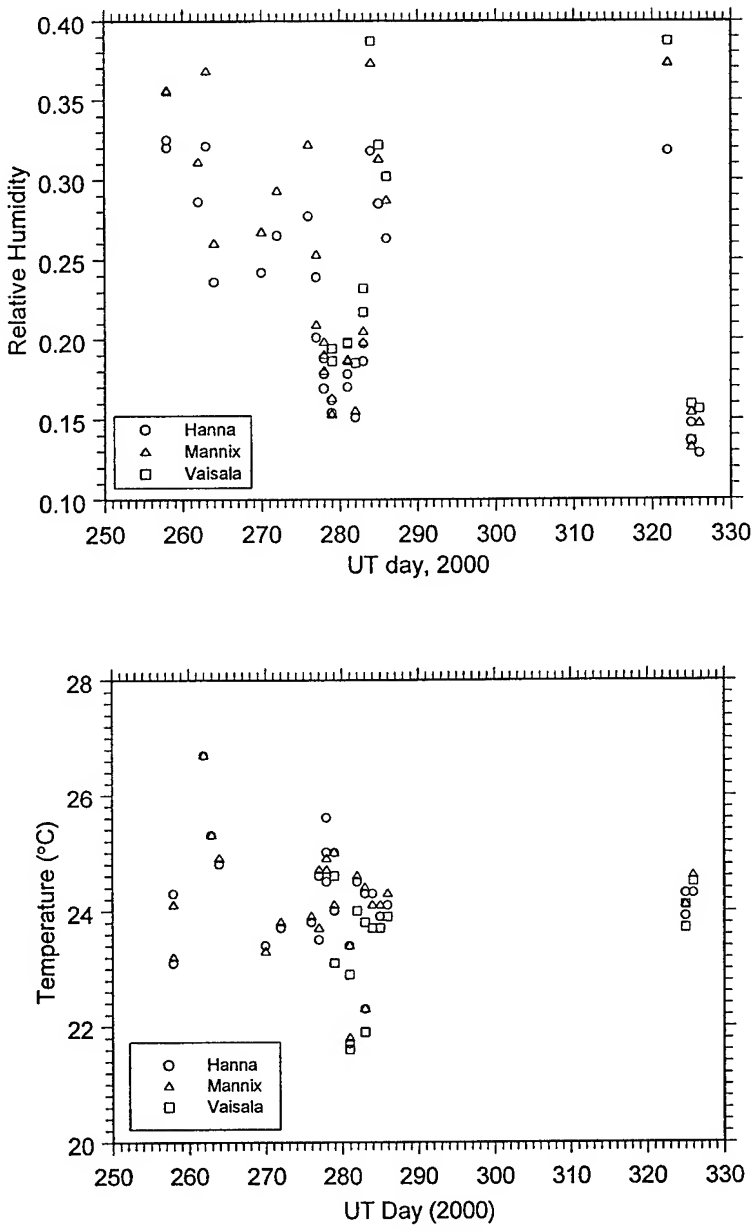

Figure 11. Relative humidity (top) and temperature (bottom) records of the three humidity/temperature sensors used in this work. The Vaisala sensor was checked against a NOAA vaisala calibration sensor and is considered to reflect true relative humidity.

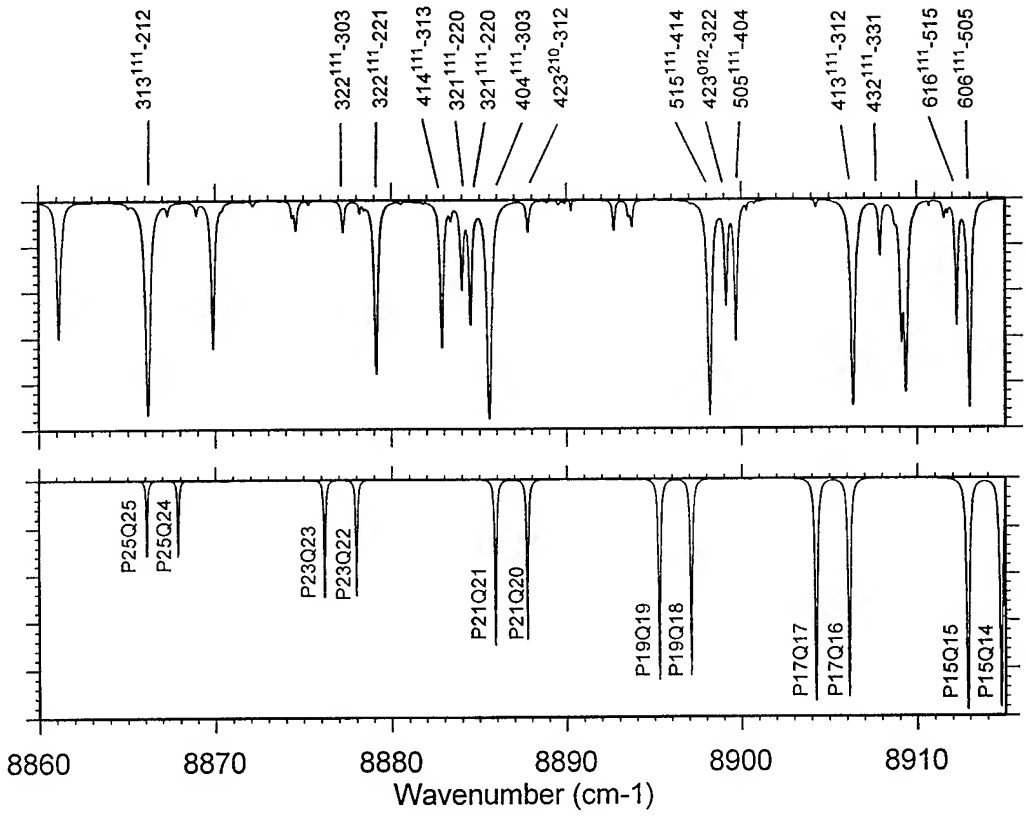

Figure 12. Predicted water vapor spectrum (top) for 55 meters horizontal path and water vapor concentration similar to levels experienced during data acquisition. The O_2 A-band ^PP branch rotational spectrum (bottom) has been numerically Raman shifted (4155 cm^{-1}) to illustrate the relationship between the Alexandrite fundamental output and corresponding Raman generated frequency.

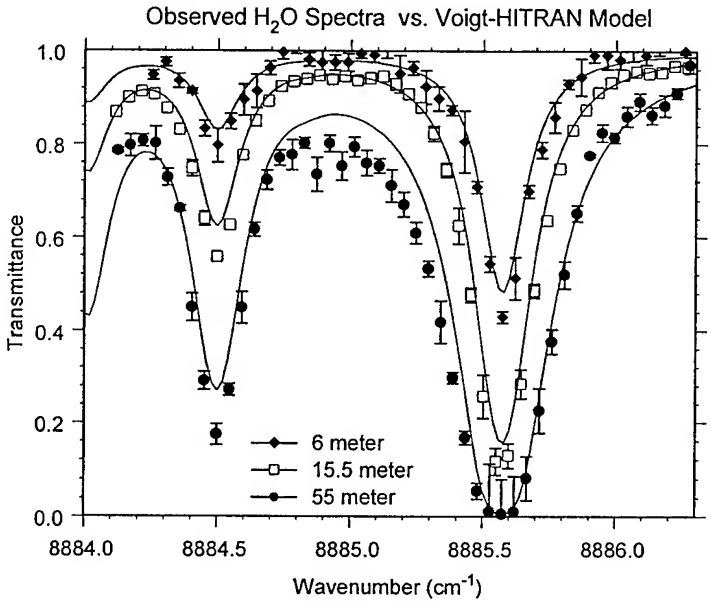

Figure 13. The measured atmospheric transmittance spectrum of water vapor near 8885 cm^{-1} for three different path lengths.

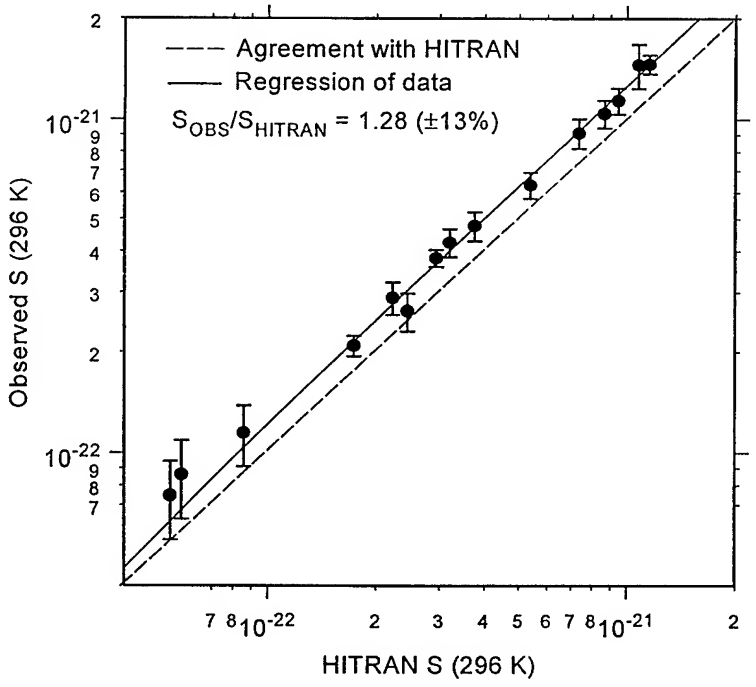

Figure 14. Measured linestrengths compared with HITRAN 2000. The solid line represents the linear regression of the data and the dashed line represents perfect agreement with HITRAN. The linear regression suggests an average 28% under-prediction of HITRAN.

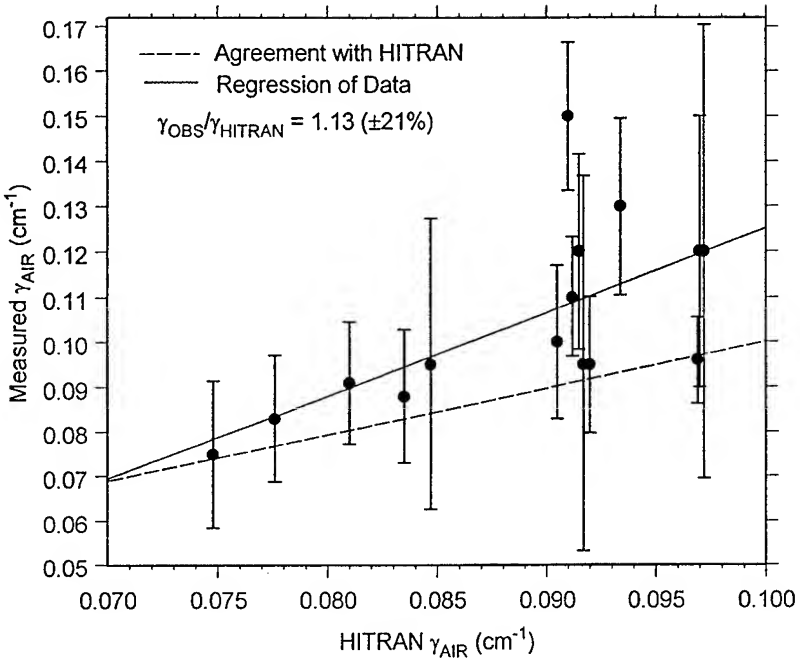

Figure 15. Measured linewidths compared with HITRAN 2000. The solid line represents the linear regression of the data and the dashed line represents perfect agreement with HITRAN. The linear regression suggests under-predicted of HITRAN widths however there appears to be a trend more under-prediction with the wider lines.

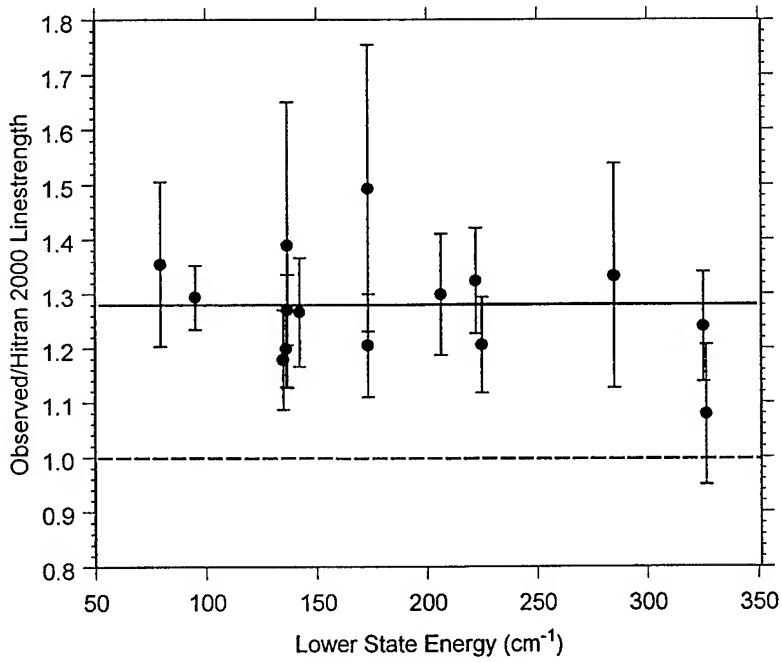

Figure 16. Measured linestrengths as a function of lower state energy.

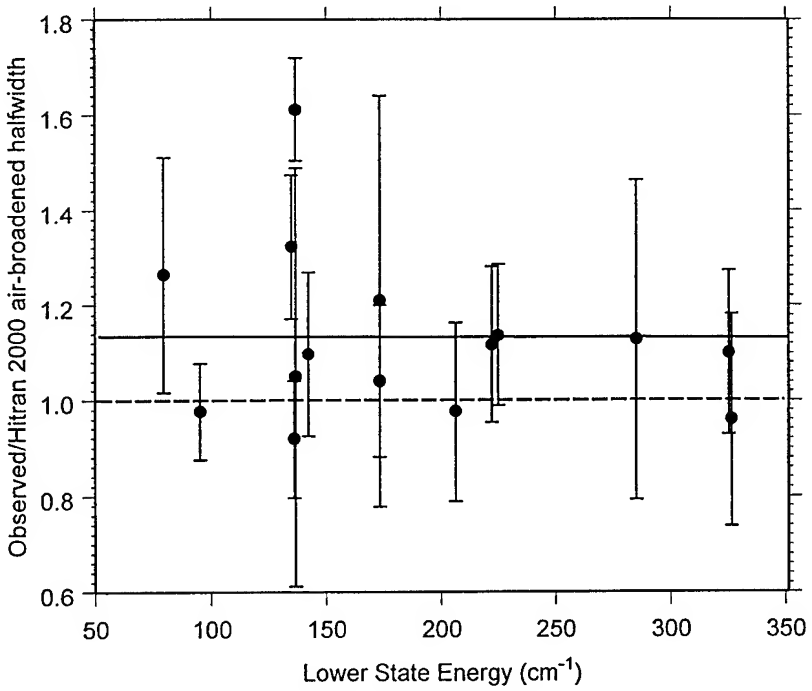

Figure 17. Measured linewidths as a function of lower state energy.

Listing of All Publications and Reports

Category (a)

"Water Vapor Line Strengths and Widths, 8865-8915 cm^{-1}", M.R. Hammond, T.D. Wilkerson, V.B. Wickwar, manuscript in preparation for *Applied Optics.*

Category (b)

"Mesospheric Temperature Observations at the USU/CASS Atmospheric Lidar Observatory (ALO)", by V.B.Wickwar, T.D. Wilkerson, M.R. Hammond, and J.P. Herron, invited paper for *Proc. 2nd Asia-Pacific Symposium on Remote Sensing*, Sendai Japan; published in SPIE 4153, paper 41,13 pp. (October 9-12, 2000).

"Water Vapor Line Strengths and Widths, 8865-8915 cm^{-1}", by Marc Hammond, Thomas D. Wilkerson, and Vincent Wickwar, presentation at Atmospheric Radiation Measurement (ARM) Science Team Meeting, Atlanta, GA (March 19-23, 2001); to be published electronically for ARM Project workshop.

"High Resolution Spectra of Atmospheric Water Vapor in the Near-IR, using a Raman-shifted Alexandrite Laser", by Marc R. Hammond, Thomas D. Wilkerson, and Vincent B. Wickwar, abstract submitted for SPIE Annual Meeting, (July 29 – August 3, 2001) San Diego, CA; to be published in SPIE *Proceedings*.

Category (e)

"Tropospheric LIDAR: Development of Techniques and Practical Measurements", graphics presentation and interim progress report on ARO Contract #DAAG 55-97-1-0297, prepared for Dr. Walter Bach (ARO) by Thomas D. Wilkerson, Vincent B. Wickwar, and Marc R. Hammond (March 2000).

"Tropospheric LIDAR: Development of Techniques and Practical Measurements", interim progress report on ARO Contract #DAAG 55-97-1-0297, prepared for Dr. Walter Bach (ARO) by Thomas D. Wilkerson, Vincent B. Wickwar, and Marc R. Hammond (January 1999).

Listing of All Participating Scientific Personnel

Principal Investigator: Thomas D. Wilkerson
Co-Investigator: Vincent B. Wickwar
Technician: Marc R. Hammond
Honors: The Co-Investigator, Prof. Wickwar, was invited to give the SPIE paper (Japan) cited above, which included the first publication of the new measurements on the near IR spectrum of atmospheric water vapor.

Inventions

Transfer of wavelength standards across spectral regions, by means of stimulated Raman scattering (application realized).

Suppression of N_2/H_2O Raman Lidar daytime background by tuning the lidar transmission to hide the Raman returns within the strongest Fraunhoffer lines (concept development).